Available online at www.sciencedirect.com
SCIENCE DIRECT®
Journal of Solid State Chemistry 178 (2005) 567–577
JOURNAL OF SOLID STATE CHEMISTRY
www.elsevier.com/locate/jssc

Spectroscopic characterization of alkaline earth uranyl carbonates

Samer Amayri[a], Tobias Reich[a,*], Thuro Arnold[b], Gerhard Geipel[b], Gert Bernhard[b]

[a]*Institute of Nuclear Chemistry, Johannes Gutenberg-Universität Mainz, Fritz-Strassmann-Weg 2, 55128 Mainz, Germany*
[b]*Forschungszentrum Rossendorf e.V., Institute of Radiochemistry, P.O. Box 510119, 01314 Dresden, Germany*

Received 14 May 2004; received in revised form 17 July 2004; accepted 28 July 2004
Available online 18 September 2004

Abstract

A series of alkaline uranyl carbonates, $M[UO_2(CO_3)_3]\cdot nH_2O$ ($M = Mg_2$, Ca_2, Sr_2, Ba_2, Na_2Ca, and CaMg) was synthesized and characterized by inductively coupled plasma mass spectrometry (ICP-MS) and atomic absorption spectrometry (AAS) after nitric acid digestion, X-ray powder diffraction (XRD), and thermal analysis (TGA/DTA). The molecular structure of these compounds was characterized by extended X-ray absorption fine-structure (EXAFS) spectroscopy and X-ray photoelectron spectroscopy (XPS). Crystalline $Ba_2[UO_2(CO_3)_3]\cdot 6H_2O$ was obtained for the first time. The EXAFS analysis showed that this compound consists of $(UO_2)(CO_3)_3$ clusters similar to the other alkaline earth uranyl carbonates. The average U–Ba distance is 3.90 ± 0.02 Å.Fluorescence wavelengths and life times were measured using time-resolved laser-induced fluorescence spectroscopy (TRLFS). The U–O bond distances determined by EXAFS, TRLFS, XPS, and Raman spectroscopy agree within the experimental uncertainties. The spectroscopic signatures observed could be useful for identifying uranyl carbonate species adsorbed on mineral surfaces.

Keywords: Uranium; Alkaline earth; Carbonate; Synthesis; Structure; Spectroscopy; EXAFS; TRLFS; XPS

1. Introduction

A number of alkaline earth uranyl carbonates have been found in nature, e.g., liebigite (CaUC), $Ca_2[UO_2(CO_3)_3]\cdot 10H_2O$, bayleyite (MgUC), $Mg_2[UO_2(CO_3)_3]\cdot 18H_2O$, andersonite (NaCaUC), $Na_2Ca[UO_2(CO_3)_3]\cdot 6H_2O$, swartzite (CaMgUC), $CaMg[UO_2(CO_3)_3]\cdot 12H_2O$, fontanite, $Ca[(UO_2)_3(CO_3)_2O_2]\cdot 6H_2O$, meta-zellerite, $Ca[UO_2(CO_3)_2]\cdot 3H_2O$, and zellerite, $Ca[UO_2(CO_3)_2]\cdot 5H_2O$ [1]. Since actinide carbonates exist over a wide range of environmental conditions [2], the last few years have seen a renewed interest in the study of uranyl carbonates in solid [3–6] and aqueous phases [7–9]. Uranyl carbonates are important for understanding the mobility of actinides in the environment. For example, recent studies of seepage waters of a mine tailing pile and mine waters of a uranium mine in Saxony, Germany, lead to the discovery of the important aqueous species $Ca_2UO_2(CO_3)_3$(aq.) [10,11]. In addition, uranyl minerals are found in soils contaminated by actinides, e.g., uranyl phosphate (meta-autonite) at the site of a former uranium processing plant at Fernald in Ohio, USA [12]. Uranyl minerals need to be considered also as important alteration phases of nuclear waste in a geological repository [13,14] or as coatings on mineral surfaces [15]. The identification of even minor amounts of such secondary uranium phases is a necessity for a better understanding of the uranium mobilization in the environment.

We report on the synthesis of the alkaline earth uranyl carbonates MgUC, CaUC, barium uranyl carbonate (BaUC), NaCaUC, and CaMgUC and their characterization by several spectroscopic techniques, i.e., time-resolved laser-induced fluorescence spectroscopy (TRLFS), extended X-ray absorption fine-structure (EXAFS) spectroscopy, and X-ray photoelectron spectroscopy (XPS). These spectroscopic techniques are non-destructive and sensitive to uranium(VI) in sample areas of a few μm^2 (TRLFS [16], micro X-ray absorption spectroscopy [17]), or allow the qualitative

*Corresponding author. Fax: +49-6131-39-24510.
E-mail address: tobias.reich@uni-mainz.de (T. Reich).

0022-4596/$ - see front matter © 2004 Elsevier Inc. All rights reserved.
doi:10.1016/j.jssc.2004.07.050

and quantitative analysis of surface layers with a thickness of a few nm (XPS [18]). The spectroscopic signatures of the alkaline earth uranyl carbonates reported here could be useful for identifying uranyl carbonate species adsorbed on mineral surfaces or formed as alteration products of nuclear waste.

2. Experimental

2.1. Synthesis of alkaline earth uranyl carbonates, $M[UO_2(CO_3)_3]\cdot nH_2O$

Many synthetic routes to alkaline earth uranyl carbonates are reported [19–23]. In this work, two methods—direct synthesis and metathesis reaction—were used for the synthesis of these compounds.

Direct synthesis: Alkaline earth uranyl carbonates were synthesized in aqueous solution by reacting stoichiometric amounts of uranyl nitrate, alkaline metal (in form of nitrate or chloride) and sodium hydrogen carbonate/sodium carbonate according to the following reaction:

$$UO_2(NO_3)_2\cdot nH_2O + 2M(NO_3)_2\cdot nH_2O + 3Na_2CO_3 \rightarrow M_2\left[UO_2(CO_3)_3\right]\cdot nH_2O + 6NaNO_3 + nH_2O \quad (1)$$

(M = divalent cation).

Metathesis reaction: The preparation of the alkaline earth uranyl carbonates was based on the double exchange reaction between magnesium, ammonium, or sodium uranyl carbonate with the alkaline metal nitrate or chloride. The weaker cation in the uranyl carbonate was displaced by an alkaline earth metal according to the following reaction:

$$(NH_4)_4UO_2(CO_3)_3 + 2M(NO_3)_2\cdot nH_2O \rightarrow M_2[UO_2(CO_3)_3]\cdot nH_2O + 4NH_4NO_3 \quad (2)$$

(M = divalent cation).

With these two methods, we were able to reproducibly synthesize the alkaline earth uranyl carbonates with high phase purity in relatively short time. Further details of the synthesis can be found in [24–26].

2.2. Chemical composition

The air-dried synthetic compounds were dissolved in 10% HNO_3 (Suprapur, Merck). The uranium content was determined using an inductively coupled plasma (Ar-plasma) mass spectrometer (ICP-MS, Elan 500, Perkin Elmer, Überlingen, Germany), whereas alkaline metal (Mg, Ca, Sr, Ba) and sodium contents were determined using a flame atomic absorption spectrometer (AAS, AAS 4100, Perkin Elmer, Überlingen, Germany). The H_2O and CO_2 contents of the air-dried samples were determined using thermogravimetric analysis (TGA) and differential thermal analysis (DTA). These two techniques were performed using a thermoanalyzer (STA 92, Setaram, Lyon, France) with the following parameters: temperature range from 20 to 1000 °C with a heating rate of 10 °C/min, oxygen flow of 3 L/h, and sample mass of about 30 mg in an aluminum crucible. The buoyancy correction for the TGA was done by measuring a blank. The reference sample for DTA was Al_2O_3.

2.3. X-ray powder diffraction

The X-ray powder-diffraction of each crystalline phase was recorded with the Universal-Röntgen-Diffraktometer (URD 6, Freiberger Präzisionsmechanik, Freiberg, Germany) using CuK_α, ($\lambda = 0.1542$ nm) at 40 kV and 30 mA. Silicon powder was used as an external standard. The diffractometer was operated in Bragg–Brentano geometry in step-mode with a step width of 0.05°. The X-ray diffraction diagrams were recorded in the 2θ range from 5° to 60°. The Diffracplus Evaluation program (Siemens) v. 2.2 [27] was used for data collection and for reflection indexing and refining. The lattice spacing d and the lattice constants a, b, and c were calculated using the program Win-Metric [28] after peak fitting of a measurement with a silicon standard.

2.4. Time-resolved laser-induced fluorescence spectroscopy

The laser pulses from a Nd-YAG laser (model DIVA II, Thales Laser, USA) were applied to the solid samples of alkaline earth uranyl carbonates where the actual laser power was monitored with an optical power meter (model 1835C, Newport, USA) to allow for corrections due to fluctuations in the laser power. The fluorescence signal was focused into a fiber optic cable that was coupled to the slit of a triple-grating spectrograph (M 1235, EG&G, USA). The fluorescence spectra were measured by a multichannel gate diode array (M 1475, EG&G) cooled to −30 °C. The spectra were collected with a controller (M 1471A, EG&G, USA). A more detailed description of the experimental setup can be found in [29]. The excitation wavelength was 266 nm. The spectra were recorded in the range from 400 to 600 nm with delay times from 0.1 to 160 μs after the application of the laser pulse. The gate time was 0.2 μs. The average laser power was 0.4 mJ. For every delay time, the fluorescence signal was averaged by sampling the single spectra over 100 laser shots. All functions (time controlling, device settings, recording of the spectra, data storage) of the spectrometer were computer controlled. The computer software GRAMS/386TM (Galactic Ind. Corp., USA) was used for the

deconvolution of the spectra. The time dependencies of the spectra were calculated with the Origin 6.1G Client (Microcal Software Inc., USA) and Excel (Microsoft Software Inc., USA) programs. The samples were measured at room temperature and a relative humidity of $60 \pm 2\%$.

2.5. Extended X-ray absorption fine-structure analysis

EXAFS measurements of solid alkaline earth uranyl carbonates were performed at the Rossendorf beam line (ROBL) at the European Synchrotron Radiation Facility (ESRF) in Grenoble, France [30,31]. At least three spectra of each sample were recorded at room and low temperatures (15–84 K) in transmission mode using a water-cooled Si(1 1 1) double-crystal monochromator. A yttrium foil was simultaneously measured for energy calibration of the spectra using the first inflection point in the derivative spectrum of the Y K edge at 17038 eV. The EXAFS oscillations were isolated from the raw, averaged data by removal of the pre-edge background, approximated by a first-order polynomial, followed by μ_0-removal via spline-fitting techniques and normalization using a Victoreen function. The ionization energy of the uranium L_{III} electron, E_0, was arbitrarily defined as 17185 eV for all averaged spectra. The EXAFS spectra were analyzed according to standard procedures using the program EXAFSPAK [32] and theoretical scattering phase and amplitude functions calculated with the ab initio program FEFF6 [33].

2.6. X-ray photoelectron spectroscopy

The uranyl carbonate samples were prepared for XPS measurements from finely dispersed powders milled in an agate mortar. A small amount of this powder was pressed into an indium foil and transferred into the spectrometer. The photoelectron spectra were measured at room temperature under a vacuum of 7×10^{-9} mbar using a custom-built XPS system (SPECS GmbH, Berlin, Germany). The photoelectron spectra were excited using the non-monochromatic K_α radiation from a high-intensity twin anode (Al/Mg) X-ray source XR-50. Due to interference of the Na and O KLL Auger lines with photoelectron lines, the photoelectron spectra were recorded both with AlK_α (1486.6 eV) and MgK_α (1253.6 eV) radiation. The photoelectrons were recorded with constant analyzer pass energy of 13 eV using the hemispherical energy analyzer PHOIBOS 100. The spectrometer resolution measured as the full-width at half-maximum of the Ag $3d_{5/2}$ line was 1.0 eV. The error of the determined binding energies was ± 0.1 eV.

3. Results and discussion

3.1. Chemical composition

According to the generic formula $M[UO_2(CO_3)_3] \cdot nH_2O$ ($M = Mg_2$, Ca_2, CaMg, Na_2Ca, Sr_2, and Ba_2), the alkaline earth uranyl carbonate samples should contain three carbonate groups, varying amounts of hydrated water, and two alkaline earth cations or, in the case of andersonite, two sodium cations and one calcium cation per one uranium atom. The results of the ICP-MS and AAS measurements showed that the atomic ratio of U to M agrees within the experimental uncertainties with the expected values (data not shown). The amount of carbonate and hydrated water was determined by thermal analysis (TGA/DTA). As shown in Table 1, three moles of CO_2 were released by one mole of sample during heating. This agrees with the generic formula of the alkaline earth uranyl carbonates. The number of water molecules in the synthetic uranyl carbonates equals 18, 10, 8, and 6 for MgUC, CaUC, SrUC, and BaUC, respectively (Table 1). These values agree with those previously reported for MgUC [34] and SrUC [23]. Our TGA/DTA measurements of CaUC showed 10 and not 11 waters as determined by Mereiter for the natural mineral liebigite [35] and agrees with earlier work [36–38]. The analytical results indicate that the synthesis of pure materials was successful. The stoichiometric formula of BaUC is $Ba_2[UO_2(CO_3)_3] \cdot 6H_2O$.

3.2. X-ray powder diffraction

Table 2 compares the lattice parameters of our synthetic uranyl carbonate powders with those for single crystals from the literature. The lattice parameters of the powders agree within the experimental error with the values reported for bayleyite [34], liebigite [35], strontium uranyl carbonate [23], andersonite [39,40], and swartzite [41]. The measured reflections of these samples were identified by matching them with the known powder diffractograms (PDF 85-970, 75-1705, 78-452, 76-2065, and 75-760).

Table 1
Results of thermogravimetric analysis (TGA) and differential thermal analysis (DTA). Moles of water and CO_2 released during heating of the synthesized samples

Formula	Temperature range (°C)	Water	CO_2
$Mg_2[UO_2(CO_3)_3] \cdot 18H_2O$	21–800	17.6 ± 0.1	3.05 ± 0.06
$Ca_2[UO_2(CO_3)_3] \cdot 10H_2O$	22–800	10.1 ± 0.2	3.43 ± 0.04
$Sr_2[UO_2(CO_3)_3] \cdot 8H_2O$	22–1002	7.96 ± 0.03	3.00 ± 0.01
$Ba_2[UO_2(CO_3)_3] \cdot 6H_2O$	22–1000	5.91 ± 0.03	2.93 ± 0.02

Table 2
Crystal data of alkaline earth uranyl carbonates. Comparison of single-crystal XRD data from the literature with powder XRD data of the synthesized samples

Name	Formula	S.G.	a (Å)	b (Å)	c (Å)	β (°)	Ref.
Bayleyite	$Mg_2[UO_2(CO_3)_3]\cdot 18H_2O$	$P2_1/a$	26.560	15.256	6.505	92.9	[34]
			26.59±0.10	15.26±0.05	6.50±0.03	92.92±0.05	This work
Liebigite	$Ca_2[UO_2(CO_3)_3]\cdot\sim 11H_2O$	*Bba2*	16.669	17.557	13.697		[35]
	$Ca_2[UO_2(CO_3)_3]\cdot 10H_2O$		16.69±0.25	17.55±0.45	13.71±0.34		This work
	$Sr_2[UO_2(CO_3)_3]\cdot 8H_2O$	$P2_1/c$	11.379	11.446	25.653	93.4	[23]
			11.33±0.16	11.41±0.14	25.62±0.42	93.53±0.20	This work
Andersonite	$Na_2Ca[UO_2(CO_3)_3]\cdot 6H_2O$	*R-3m*	17.902		23.734		[39]
			17.904		23.753		[40]
			17.889±0.007		23.739±0.005		This work
Swartzite	$CaMg[UO_2(CO_3)_3]\cdot 12H_2O$	$P2_1/m$	11.080	14.634	6.439	99.4	[41]
			11.084±0.005	14.601±0.008	6.436±0.006	99.59±0.07	This work

S.G.—space group.

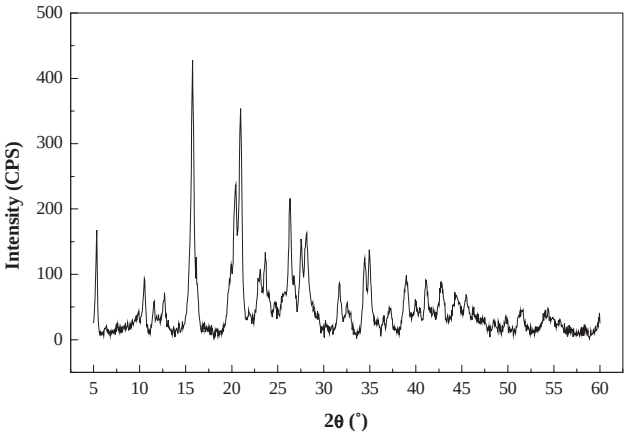

Fig. 1. Powder diffraction pattern of barium uranyl carbonate $Ba_2[UO_2(CO_3)_3]\cdot 6H_2O$.

We recorded for the first time the X-ray diffraction diagram of a BaUC powder (Fig. 1). Unfortunately, the signals of the recorded peaks were insufficient to get exact information about the crystal structure of BaUC. However, the indexed X-ray reflections are inconsistent with those reported for the starting materials or barium carbonate. Up to now, the international diffraction database (JCPDS) does not have any data on the crystal structure of BaUC. Therefore, we investigated the structure of BaUC by EXAFS to determine the metrical parameters of the uranium neighbors.

All samples were stored in air at normal humidity (60%) for 1 year. The same X-ray diffraction patterns were recorded before and after storage. This indicates a good storage or weathering stability of the synthesized compounds under these conditions. Note that the uranyl carbonates start liberating water at approximately 40 °C as observed in the TGA/DTA measurements.

3.3. Extended X-ray absorption fine-structure analysis

EXAFS measurements provide element-specific short-range structural and chemical information on the uranium(VI) coordination environment including identities and coordination numbers of the neighboring atoms and bond distances to them. We used this technique to compare the metrical parameters of the local coordination environment of uranium in alkaline earth uranyl carbonates with the structural information available from single-crystal XRD analysis. One important aspect of this EXAFS study was to explore the possibility of detecting the alkaline earth metal in the uranium near-neighbor environment. All samples were measured at low temperature in the range of 15–84 K to reduce thermal vibrations and to enhance the corresponding contribution of these atoms to the EXAFS amplitude. In case of BaUC, whose crystal structure is

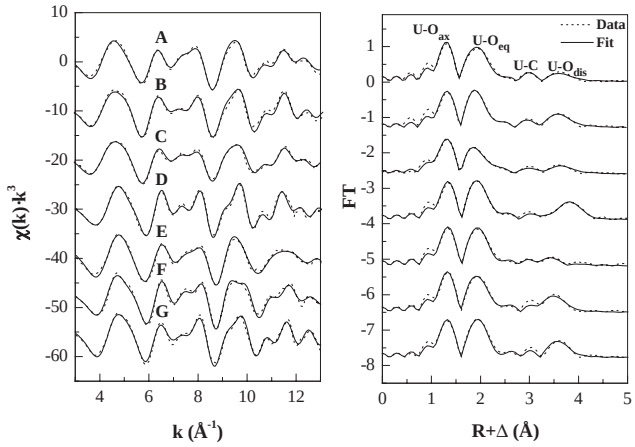

Fig. 2. Left: Raw uranium L_{III}-edge k^3-weighted EXAFS spectra of solid alkaline earth uranyl carbonates: (A) MgUC (84 K), (B) CaUC (26 K), (C) natural liebigite (room temperature), (D) SrUC (16 K), (E) BaUC (15 K), (F) NaCaUC (30 K), and (G) CaMgUC (30 K). Right: corresponding Fourier transform magnitudes without phase correction.

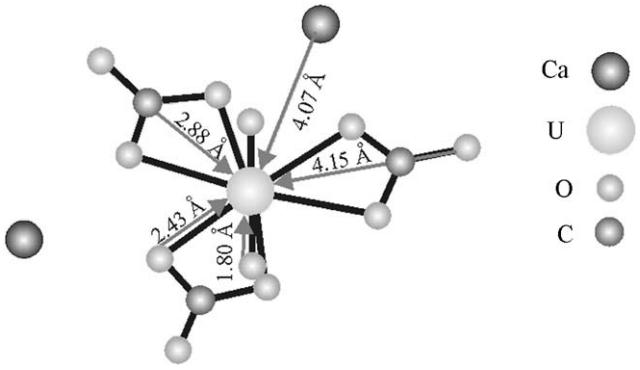

Fig. 3. Ball-and-stick drawing illustrating the structural model used for fitting the EXAFS spectra. Adapted from single-crystal XRD data of liebigite [35].

unknown, its EXAFS structural parameters can be compared to the alkaline earth uranyl carbonates with known crystal structures. The raw uranium L_{III}-edge k^3-weighted EXAFS spectra of all samples together with the best fit to the data and their corresponding Fourier transforms (FTs) are shown in Fig. 2. Note that the FTs are uncorrected for scattering phase shifts ($R+\Delta$) causing peaks to appear at shorter distances. The EXAFS spectra of all solids show similar oscillations indicating similar uranium near-neighbor surroundings. Some differences in the EXAFS pattern are reflected in the FTs in the range of 3–4 Å. The scattering interactions with the distal oxygen atom, O_{dis}, of the CO_3^{2-} group and the alkaline earth metal are expected in this range.

The alkaline earth uranyl carbonates of this study contain isolated clusters of the composition $(UO_2)(CO_3)_3$ [23,34,35,39–41] (Fig. 3). The atoms of this cluster, i.e., axial and equatorial oxygens, O_{ax} and O_{eq}, carbon and O_{dis}, give rise to the FT peaks centered at approximately 1.3, 2.0, 2.8, and 3.7 Å, respectively. The intensity of the O_{ax} and O_{eq} peaks is the same for all samples measured at low temperature. The influence of the temperature on the FT peak intensity at 3.7 Å can be seen for CaUC. This compound was measured at room temperature (natural liebigite, sample C in Fig. 2) and at 26 K (synthetic CaUC, sample B in Fig. 2). As one would expect, the FT peak intensity increases due to a reduced Debye–Waller factor caused by the temperature decrease. The same temperature effect was observed for MgUC and SrUC (data not shown). By comparing the FT magnitudes around 3.7 Å of MgUC and CaUC measured at low temperatures, i.e., spectra A and B in Fig. 2, one can conclude that the higher intensity in case of CaUC indicates the presence of calcium at this distance. It is known from single-crystal XRD that MgUC does not have any U or Mg atoms at distances up to 5 Å [34]. Therefore, EXAFS spectrum A in Fig. 2 represents the isolated cluster $(UO_2)(CO_3)_3$. The presence of Sr in SrUC leads to a significant increase and slight shift toward higher R values of the FT peak centered at 3.7 Å (see D in Fig. 2) as compared to the other uranyl carbonates. Also, spectra F and G of NaCaUC and CaMgUC, respectively, show a larger FT magnitude at approximately 3.7 Å indicating the presence of metal atoms. Surprisingly, the FT of BaUC at 15 K does not show any significant intensity in the FT range of the O_{dis} atom (see curve E in Fig. 2). The EXAFS analysis described below revealed that the U–O_{dis} multiple-scattering (MS) contribution interferes destructively with the U–Ba single-scattering (SS) contribution.

The calculation of the best theoretical fit to the raw EXAFS data shown in Fig. 2 included two steps. In the first step, we assumed the $(UO_2)(CO_3)_3$ cluster as a structural model (see Fig. 3) and fitted the raw EXAFS data with the U–O_{ax}, U–O_{ax}, U–C SS, and U–O_{ax} MS paths. The U–O_{ax} MS interaction was modeled without introducing any additional adjustable parameters by the three-legged MS path along the linear UO_2^{2+} unit according to [42]. The coordination numbers of the O_{ax}, O_{eq}, and C shells for all samples were 2.0 ± 0.2, 6.5 ± 0.6, and 3.4 ± 0.5, respectively, and agree with the formation of $(UO_2)(CO_3)_3$ clusters. The second step aimed at determining the structural parameters of the O_{dis} and M shells. To be more sensitive in the fit to these minor components, we isolated the O_{dis} and M scattering contributions from the raw data according to the difference technique [43]. Briefly, the theoretical fit obtained in the first step was subtracted from the raw data followed by Fourier filtering of the residual in the R range of 2.0–4.5 Å. The residual EXAFS was modeled

using the SS path U–M (M = Ca, Sr, Ba) and the three-legged MS paths U–C–O_{dis} and U–C–O_{eq}. For the final fit to the raw data, the coordination numbers of all shells were held constant at the values determined during the previous two modeling steps. The results are presented in Fig. 2 and summarized and compared to single-crystal XRD data in Table 3. The average distances between U and O_{ax}, O_{eq}, and C atoms in all alkaline earth uranyl carbonates are identical and equal 1.79–1.80, 2.43–2.45, and 2.88–2.90 Å, respectively. For the more distant U–O_{dis} shell, the range of bond distances is somewhat larger, i.e., 4.15–4.21 Å. The oxygen and carbon distances agree well with the XRD values (Table 3) for MgUC [34], CaUC [35], SrUC [23], NaCaUC [39,40], and CaMgUC [41]. The EXAFS metrical parameters of BaUC indicate that this compound consists of $(UO_2)(CO_3)_3$ clusters similar to the other alkaline earth uranyl carbonates.

As expected from the crystal structure, the EXAFS analysis of MgUC did not show any evidence of Mg or U. The low-temperature measurement of CaUC clearly showed the presence of two Ca atoms at a distance of 4.05 ± 0.02 Å. As we reported in our previous study of the $[UO_2(CO_3)_3]^{4-}$(aq.) and $Ca_2UO_2(CO_3)_3$(aq.) species and natural and synthetic liebigite, the detection of the U–Ca interaction is less certain in case of room-temperature measurements [9]. An equally good fit to the EXAFS could be obtained without including the U–Ca shell. The low-temperature EXAFS measurements of NaCaUC and CaMgUC detected Ca atoms at distances of 3.95 ± 0.02 and 4.03 ± 0.02 Å. These values agree with the corresponding U–Ca distances of 3.96 and 4.03 Å calculated from the single-crystal XRD data [40,41]. It should be noted that we did not attempt to detect the position of Na atoms in NaCaUC since Ca is a stronger scattering atom than Na and occurs at nearly the same distance (see Table 3). Two Sr atoms at a distance of 4.26 ± 0.02 Å were detected in SrUC at low temperature. In contrast to CaUC, the presence of Sr in SrUC at 4.28 ± 0.02 Å was clearly detectable in the EXAFS spectrum even at room temperature (data not shown). The reason is the increase of the scattering amplitude with increasing atomic number, e.g., Ca, Sr, and Ba. In case of BaUC, the least-squares fit of the EXAFS spectrum measured at 15 K resulted in 0.7 ± 0.1 Ba atoms at a distance of 3.90 ± 0.02 Å. This distance is significantly shorter compared to the average U–M distances of 4.05 ± 0.02 and 4.26 ± 0.02 Å in CaUC and SrUC, respectively (Table 3). This, together with the detection of six water molecules in BaUC, allows to conclude that the position of the Ba cation relative to the $(UO_2)(CO_3)_3$ cluster in the BaUC crystal is different from the positions of Mg, Ca, and Sr cations in MgUC, CaUC, and SrUC, respectively.

Table 3
EXAFS structural parameters of solid alkaline earth uranyl carbonates and comparison with single-crystal XRD data

Symbol	Formula	$2 \times (U–O_{ax})$		$6 \times (U–O_{eq})$		$3 \times (U–C)$		$3 \times (U–O_{dis})$		$N \times (U–M^{2+})$		
		R (Å)	σ^2 (Å^2)	R (Å)	σ^2 (Å^2)	R (Å)	σ^2 (Å^2)	R (Å)	σ^2 (Å^2)	N	R (Å)	σ^2 (Å^2)
MgUC	$Mg_2[UO_2(CO_3)_3] \cdot 18H_2O$	1.80	0.002	2.45	0.004	2.90	0.003	4.20	0.003	—	—	—
	XRD [34]	1.79		2.44		2.89		4.13		—	—	
CaUC	$Ca_2[UO_2(CO_3)_3] \cdot 10H_2O$	1.80	0.002	2.43	0.003	2.88	0.001	4.15	0.005	2	4.05	0.002
	natural liebigite [9]	1.80	0.002	2.43	0.006	2.88	0.003	4.17	0.002	2	4.04	0.014
	XRD [35]	1.78		2.43		2.86		4.11		2	4.07	
SrUC	$Sr_2[UO_2(CO_3)_3] \cdot 8H_2O$	1.81	0.001	2.43	0.004	2.90	0.001	4.16	0.001	2	4.26	0.002
	XRD [23]	1.78		2.43		2.87		4.10		2	4.23	
BaUC	$Ba_2[UO_2(CO_3)_3] \cdot 6H_2O$	1.81	0.002	2.44	0.004	2.89	0.002	4.19	0.005	1	3.90	0.002
NaCaUC	$Na_2Ca[UO_2(CO_3)_3] \cdot 6H_2O$	1.79	0.002	2.43	0.004	2.88	0.002	4.15	0.003	2	3.95	0.003
	XRD [40]	1.78		2.44		2.88		4.12		$2Ca^{2+}$	3.96	
										$1Na^{+}$	3.80	
										$1Na^{+}$	4.17	
CaMgUC	$CaMg[UO_2(CO_3)_3] \cdot 12H_2O$	1.79	0.002	2.44	0.003	2.90	0.001	4.21	0.005	1	4.03	0.002
	XRD [41]	1.78		2.44		2.88		4.03		$1Ca^{2+}$	4.03	

The coordination numbers N were held constant at the value obtained in a previous fit with variable parameters. Error in distance R equals ± 0.02 Å. σ^2 Debye–Waller factor. The distances R reported for single-crystal XRD were averaged. All samples were measured at low temperatures (15–84 K), except natural liebigite, which was measured at room temperature. The distances U–M were calculated from the XRD data up to 5 Å.

3.4. Time-resolved laser-induced fluorescence spectroscopy

We studied the fluorescence properties of the synthetic uranyl carbonates to contribute toward a database of secondary uranium phases that may form in areas contaminated by uranium. The TRLFS data may provide a link between the fluorescence properties of minerals and possible unknown ternary uranium(VI) complexes in environmental waters. There is little spectral information on such species available in the literature.

The data for the main fluorescence emissions of the solid alkaline earth uranyl carbonates in comparison with those of the aqueous uranyl ion [16] and the uranyl triscarbonato species [10] are listed in Table 4. Fig. 4 shows the fluorescence spectra of all synthesized compounds.

In contrast to the room temperature non-fluorescent $[UO_2(CO_3)_3]^{4-}$(aq.) species, all solid alkaline earth uranyl carbonates show intensive fluorescence emission bands (Fig. 4). We found a bathochromic shift up to 5.0 nm in the fluorescence emissions between these solid samples. The fluorescence lifetimes range from 16 to 145 μs. The fluorescence emissions bands at 465.4, 482.9, 502.7, 524.5, 545.4, and 571.5 nm of synthetic CaUC agree with fluorescence emissions of the mineral liebigite from the Mineralogical Collection of the Technische Universität Bergakademie Freiberg, Germany (Swartswalder Mine, Golden, CO, USA).

Six intensive fluorescence emission bands for the natural andersonite sample (from Mineralogical Collection of the Technische Universität Bergakademie Freiberg, Germany; Honeybee No. 2 Mine, Cane Springs Canyon, San Juan Co., UT, USA) at 468.4, 485.2, 504.8, 526.2, 549.6, and 575.4 nm were detected, which agree with the fluorescence emission bands of synthetic andersonite. The respective lifetime of 33 ± 4 μs, which was calculated from the TRLFS spectra of the natural andersonite sample, was slightly less than the one obtained for the synthesized sample. This small discrepancy in lifetime between the synthesized and the natural andersonite sample could be attributed to a minor contamination in the natural andersonite sample. For example, minor amounts of Fe decrease the fluorescence lifetime [44].

The maxima of the fluorescence emissions related to the radiation emitting level corresponding to 20502 cm^{-1} for UO_2^{2+} in perchlorate medium [45] can be used for calculating the vibrational frequencies of the ground state [46]. Four maxima of the fluorescence emission in the range of approximately 485–550 nm were used to calculate the band spacings listed in Table 4. The emission band to the highest exited state of the ground state vibrational level (~570 nm) was not included in this calculation due to its low intensity (see Fig. 4). For

Table 4
Spectroscopic properties of the solid alkaline earth uranyl carbonates studied by TRLFS

Symbol	Formula	Fluorescence emission bands (nm)						Lifetime (μs)	Band spacing (cm^{-1})	$U–O_{ax}$ (pm)
MgUC	$Mg_2[UO_2(CO_3)_3]\cdot 18H_2O$	471.3	487.7	506.9	527.6	551.4	578.3	17.9 ± 0.5	789 ± 25	182 ± 3
CaUC	$Ca_2[UO_2(CO_3)_3]\cdot 10H_2O$	465.4	482.9	502.7	524.5	545.4	571.5	145 ± 5	791 ± 53	182 ± 6
	natural liebigite	466.9	483.1	502.7	524.1	545.9	571.9	313 ± 10	794 ± 28	182 ± 3
SrUC	$Sr_2[UO_2(CO_3)_3]\cdot 8H_2O$	482.5	488.8	502.8	522.9	545.4	569.2	77 ± 1	777 ± 17[a]	184 ± 2
BaUC	$Ba_2[UO_2(CO_3)_3]\cdot 6H_2O$	469.9	487.7	507.3	528.9	552.2	570.5	16.3 ± 0.4	798 ± 6	181 ± 1
NaCaUC	$Na_2Ca[UO_2(CO_3)_3]\cdot 6H_2O$	470.6	486.1	505.4	526.7	549.6	573.9	65.2 ± 0.6	792 ± 7	182 ± 1
	natural andersonite	486.4	485.2	504.8	526.2	549.6	575.4	33 ± 4	805 ± 4	181 ± 1
CaMgUC	$CaMg[UO_2(CO_3)_3]\cdot 12H_2O$	472.3	488.9	509.2	531.0	554.7	578.9	59.4 ± 0.1	809 ± 6	180 ± 1
	UO_2^{2+}(aq.), pH 1.0	471.3	488.9	510.5	533.9	559.4	585.5	1.8 ± 0.8	859 ± 6	175 ± 1
	$[UO_2(CO_3)_3]^{4-}$(aq.)	No uranium fluorescence at 25 °C								

Comparison with UO_2^{2+} [16] and $[UO_2(CO_3)_3]^{4-}$ [10] ions in aqueous solutions. The experimental error in the fluorescence emission bands equals ±1 nm.
[a]Only three peaks considered (see text).

SrUC, also the transition to the ground state (488.8 nm) has a low intensity resulting in a larger error of the maximum of the fluorescence emission band. Therefore, the calculation of the band spacing in SrUC included only the emission band maxima at 502.8, 522.9, and 545.4 nm. As can be seen from Table 4, the vibrational levels of the ground state, which are related to the symmetric stretching vibration v_1 of UO_2^{2+}, are separated by approximately 777–805 cm^{-1}. We also used Raman spectroscopy to measure the v_1 vibration. The following values were obtained for MgUC, CaUC, SrUC, and BaUC: 822, 826, 812, and 818 $\pm$ 4 cm^{-1}, respectively [24]. Using the empirical relation between the U–O_{ax} bond length R_{UO} and v_1 [47]:

$$R_{UO}/(pm) = 10650[v_1/(cm^{-1})]^{-2/3} + 57.5, \quad (3)$$

we obtained the following values using TRLFS (Raman): MgUC 182 (179) pm, CaUC 182 (179) pm, SrUC 184 (180) pm, BaUC 181 (179) pm, NaCaUC 182 pm, and CaMgUC 180 pm (Table 4). The error in bond length determined by Raman spectroscopy equals $\pm$0.4 pm. For the error using TRLFS, refer to Table 4. The U–O_{ax} bond lengths of the alkaline earth uranyl carbonates are in the range of 1.79–1.82 Å. These values agree with the results of our EXAFS measurements (Table 3). The U–O_{ax} bond length of the aqueous UO_2^{2+} ion determined by TRLFS is significantly shorter, i.e., 1.75 Å (Table 4). As shown in a previous study of uranium(VI) minerals [16], TRLFS can be used for determining U–O_{ax} bond distances in solids.

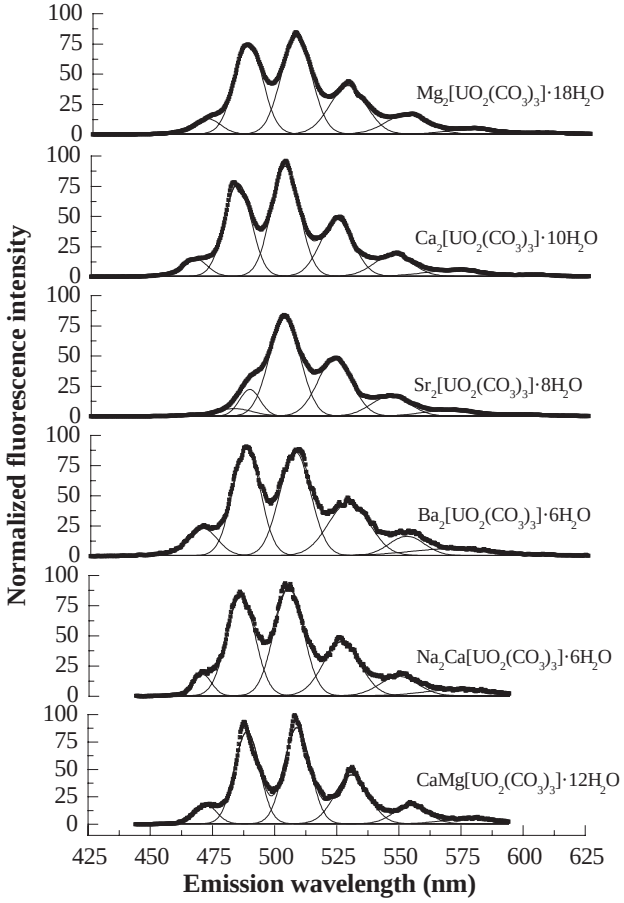

Fig. 4. Fluorescence spectra of synthetic alkaline earth uranyl carbonates (solid lines show the curve fit of the spectra using a Gaussian line shape). The TRLFS spectra were recorded at room temperature.

3.5. X-ray photoelectron spectroscopy

We studied the electronic structure of the alkaline earth uranyl carbonates by core-level and valance-level XPS. Table 5 summarizes the measured electron binding energies of the C 1*s*, O 1*s*, U 4*f* levels together with the most intense XPS peaks of the alkaline earth elements, i.e., Mg 2*p*, Ca 2*p*, Sr 3*p*, and Ba 3*d*. Not all samples showed a C 1*s* signal due to adventitious carbon on the surface that could be used as a reference to correct the measured binding energies for electrostatic sample charging. Therefore, we corrected for the sample charging by setting the binding energy of C 1*s* electrons of CO_3^{2-} equal to 289.6 eV. The measured binding energies are compared to those of $K_4UO_2(CO_3)_3$ [48] and our results for $MgCO_3$ and $CaCO_3$ (see Table 5). The binding energies of O 1*s*, Na 1*s*, U 4*f* and the

Table 5
Electron binding energies (eV) of synthetic alkaline earth uranyl carbonates and comparison with reference samples $K_4UO_2(CO_3)_3$ [48], $MgCO_3$, and $CaCO_3$

Symbol	Formula	O 1*s*	U 4$f_{7/2}$	U 4$f_{5/2}$	Mg 2*p*	Ca 2$p_{3/2}$	Ca 2$p_{1/2}$	Sr 3$p_{1/2}$	Sr 3$p_{3/2}$	Ba 3$d_{5/2}$	Ba 3$d_{3/2}$	Na 1*s*
MgUC	$Mg_2[UO_2(CO_3)_3]\cdot 18H_2O$	531.7	381.9	392.8	50.2							
CaUC	$Ca_2[UO_2(CO_3)_3]\cdot 10H_2O$	531.8	381.8	392.8		347.5	351.1					
SrUC	$Sr_2[UO_2(CO_3)_3]\cdot 8H_2O$	531.7	382.0	392.9				279.8	269.4			
BaUC	$Ba_2[UO_2(CO_3)_3]\cdot 6H_2O$	531.6	381.6	392.5						780.5	795.8	
NaCaUC	$Na_2Ca[UO_2(CO_3)_3]\cdot 6H_2O$	531.6	382.2	393.0		347.4	350.9					1071.7
MgCaUC	$CaMgUC[UO_2(CO_3)_3]\cdot 12H_2O$	531.7	381.7	392.6	50.2	347.4	351.0					
	$K_4UO_2(CO_3)_3$	531.4	382.1	392.9								
	$MgCO_3$	531.7			49.9							
	$CaCO_3$	531.5				347.1	350.7					

The binding energy of C 1*s* of the CO_3^{2-} group was taken as 289.6 eV to correct for sample charging. Error in electron binding energy equals $\pm$0.1 eV.

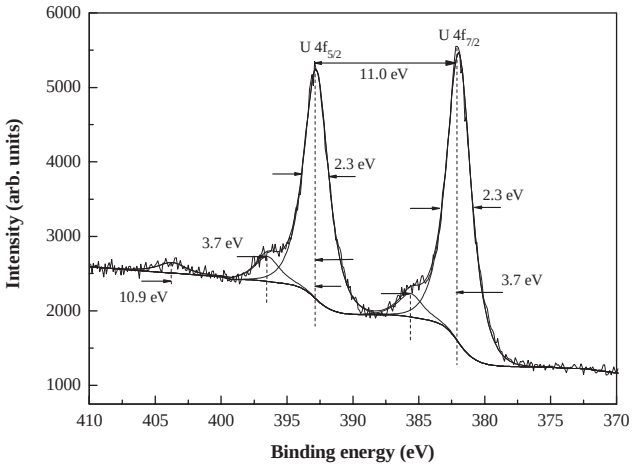

Fig. 5. X-ray photoelectron spectrum of U 4*f* electrons of synthetic $Ca_2[UO_2(CO_3)_3]\cdot 10H_2O$. The spectra were corrected for MgK_α satellites due to non-monochromatic excitation.

corresponding XPS lines of the alkaline earth metals in the uranyl carbonates agree with those of the reference samples. The comparison of these electron binding energies indicates the presence of UO_2^{2+} and CO_3^{2-} groups as well as of divalent alkaline earth metals at all sample surfaces.

Fig. 5 shows the U 4*f* spectrum of synthetic CaUC, which is representative for all uranyl carbonate samples. The observed spin-orbit splitting between the U $4f_{7/2}$ and $4f_{5/2}$ levels of 11.0 eV is constant for the entire series of alkaline earth uranyl carbonates (Table 5). In addition, shake-up satellites with a relative intensity of 8–11% appear at 3.7 eV toward higher binding energy of the U $4f_{7/2}$ and U $4f_{5/2}$ line, respectively (Fig. 5). These observations are characteristic for U(VI). For example, Teterin et al. reported for a series of uranyl compounds that the shake-up satellites have a higher binding energy of approximately 3–4 eV compared to the main U 4*f* lines [48]. The average U 4*f* spin-orbit splitting was 10.9 eV. This agrees with our results.

The XPS spectra of the alkaline earth uranyl carbonates from 0–35 eV binding energy are shown in Fig. 6. The most intense features are due to the valance molecular orbitals (VMO) centered at approximately 5 eV and the various alkaline earth metal lines (Ba 5*p*, Sr 4*p*, and Ca 3*p*). There are also some features with less intensity that deserve special attention. All alkaline earth uranyl carbonates show two distinct peaks at approximately 9 and 12 eV binding energy (see Fig. 6). These peaks originate from the molecular orbitals of the CO_3^{2-} group as it was shown in the XPS spectra of Th(IV) compounds with ligands of D_{3h} symmetry (NO_3^- and CO_3^{2-}) [48]. Two additional weak structures in the region of 15–20 eV can be seen in the spectra of MgUC, NaCaUC, CaMgUC, and CaUC (Fig. 6). These features are inner valence molecular orbitals (IVMO) related to the U $6p_{3/2}$ electrons. In a $[UO_2^{2+}O_6]^{10-}$ cluster with the

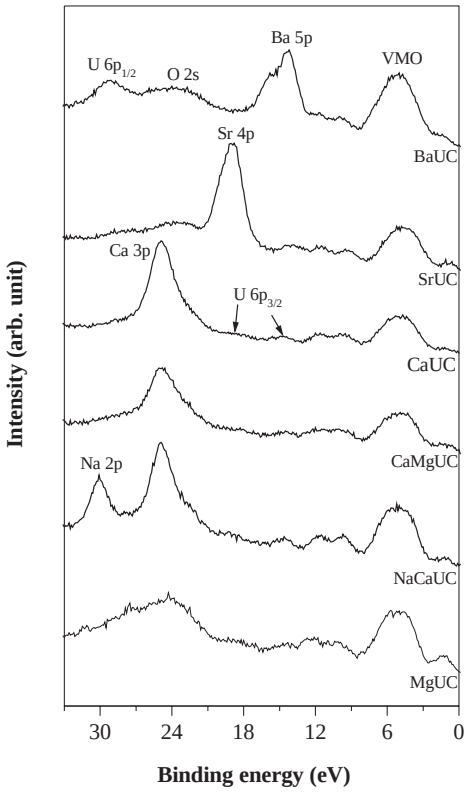

Fig. 6. X-ray photoelectron spectra of valence electrons of synthetic alkaline earth uranyl carbonates. The spectra were corrected for MgK_α satellites due to non-monochromatic excitation.

D_{6h} point symmetry, these IVMO's are assigned as $2a_{2u}$ and $2e_{1u}$. The energy difference ΔE between $2a_{2u}$ and $2e_{1u}$ is approximately 4.6 eV. Using the relationship between ΔE and the U–O_{ax} and U–O_{eq} bond distances between uranium and its axial and equatorial oxygen atoms, it is possible to calculate these bond distances from the measured ΔE value [49]. For ΔE equal 4.6 eV, the calculated U–O_{ax} and U–O_{eq} bond distances are 1.71 and 2.42 Å, respectively. Within the experimental uncertainties of approximately 5%, these values agree with the average bond distances of 1.80 and 2.43 Å measured by EXAFS (see Table 3).

4. Conclusion

Crystalline $Ba_2[UO_2(CO_3)_3]\cdot 6H_2O$ was synthesized and characterized for the first time. Although the crystallinity of our sample precluded the determination of metrical parameters of the crystal lattice by powder XRD, uranium L_{III}-edge EXAFS spectroscopy showed that BaUC consists of $(UO_2)(CO_3)_3$ clusters as known for the other uranyl carbonates $M[UO_2(CO_3)_3]\cdot nH_2O$ (M = Mg_2, Ca_2, Sr_2, Na_2Ca, and CaMg). In addition, approximately one Ba cation is located at a distance of 3.90 ± 0.02 Å from the center of this cluster. The presence of M (M = Ca, Sr, and Ba) at a distance of

approximately 4 Å from uranium in the structure of the uranyl carbonates could be identified due to their electron-scattering characteristics using low-temperature EXAFS spectroscopy.

TRLFS measurements revealed identical fluorescence emission bands between the synthetic alkaline earth uranyl carbonate and the corresponding natural sample. Distinct differences either in the maxima of the fluorescence emission band or the lifetimes between different uranyl carbonates can be used to distinguish them. In particular, TRLFS could be used for the speciation of uranium(VI) secondary carbonate phases formed on mineral surfaces or as a result of alterations of nuclear waste. This analysis of solids could be complemented by XPS, an element-specific, non-destructive, and direct probe for the first few nanometers of a surface. The surface composition as determined by XPS could assist the interpretation of the TRLFS or other spectroscopic measurements. Finally, the well-characterized substances can be used to determine their up to now unknown solubility. The spectroscopic properties reported in this study provide the basis for identifying these compounds before and after solubility studies using TRLFS, EXAFS, and XPS [50].

Acknowledgments

We thank U. Schaefer, A. Scholz (both FZR), and J. Drebert (JOGU) for the support of the ICP-MS, XRD, and XPS measurements, respectively. We gratefully acknowledge the help of H. Funke, C. Hennig, A. Roßberg, and A. Scheinost with the EXAFS experiments, which were performed at BM20 (ROBL) at the ESRF. A. Massanek (TU Bergakademie Freiberg) provided the uranium mineral samples.

References

[1] J.A. Mandarino, M.E. Black, Fleischer's Glossary of Mineral Species 2004, The Mineralogical Record Inc., Tucson, 2004.
[2] D.L. Clark, D.E. Hobart, M.P. Neu, Chem. Rev. 95 (1995) 25–48.
[3] Y.P. Li, P.C. Burns, Can. Mineral. 39 (2001) 1147–1151.
[4] Y.P. Li, S.V. Krivovichev, P.C. Burns, Mineral. Mag. 65 (2001) 297–304.
[5] Y.P. Li, P.C. Burns, J. Solid State Chem. 166 (2002) 219–228.
[6] K.A. Hughes, P.C. Burns, Am. Mineral. 88 (2003) 962–966.
[7] P.G. Allen, J.J. Bucher, D.L. Clark, N.M. Edelstein, S.A. Ekberg, J.W. Gohdes, E.A. Hudson, N. Kaltsoyannis, W.W. Lukens, M.P. Neu, P.D. Palmer, T. Reich, D.K. Shuh, C.D. Tait, B.D. Zwick, Inorg. Chem. 34 (1995) 4797–4807.
[8] G. Geipel, G. Bernhard, V. Brendler, H. Nitsche, Radiochim. Acta 82 (1998) 59–62.
[9] G. Bernhard, G. Geipel, T. Reich, V. Brendler, S. Amayri, H. Nitsche, Radiochim. Acta 89 (2001) 511–518.
[10] G. Bernhard, G. Geipel, V. Brendler, H. Nitsche, Radiochim. Acta 74 (1996) 87–91.
[11] G. Bernhard, G. Geipel, V. Brendler, H. Nitsche, J. Alloys Comp. 271 (1998) 201–205.
[12] E.C. Buck, N.R. Brown, N.L. Dietz, Environ. Sci. Technol. 30 (1996) 81–88.
[13] R.J. Finch, R.C. Ewing, J. Nucl. Mater. 190 (1992) 133–156.
[14] E.C. Pearcy, J.D. Prikryl, W.M. Murphy, B.W. Leslie, Appl. Geochem. 9 (1994) 713–732.
[15] A. Boughriet, L. Gengembre, J. Laureyns, P. Recourt, H.R. Langelin, A. Nacer, Phys. Chem. Chem. Phys. 2 (2000) 1059–1068.
[16] G. Geipel, G. Bernhard, M. Rutsch, V. Brendler, H. Nitsche, Radiochim. Acta 88 (2000) 757–762.
[17] P.M. Bertsch, D.B. Hunter, S.R. Sutton, S. Bajt, M.L. Rivers, Environ. Sci. Technol. 28 (1994) 980–984.
[18] D. Briggs, J.T. Grant, Surface Analysis by Auger and X-ray Photoelectron Spectroscopy, IM Publications, Chichester, 2003.
[19] J.M. Axelrod, F.S. Grimaldi, C. Milton, K.J. Murata, Am. Mineral. 36 (1951) 1–22.
[20] M. Bachelet, E. Chelyan, M. Douis, J.C. Goulette, Bull. Soc. Chim. France 19 (1952) 565–569.
[21] R. Meyrowiz, M.L. Lindberg, US Geol. Survey Prof. Pap. 400-B (1960) B440–B441.
[22] R. Meyrowiz, D.R. Ross, A.D. Weeks, US Geol. Survey Prof. Pap. 475-B (1963) B162–B163.
[23] K. Mereiter, Acta Crystallogr. C 42 (1986) 1678–1681.
[24] S. Amayri, Synthese, Charakterisierung und Löslichkeit von Erdalkaliuranylcarbonaten $M_2[UO_2(CO_3)_3]\cdot xH_2O$; M: Mg, Ca, Sr, Ba, Ph.D. Thesis, Technische Universität Dresden, Dresden, 2002.
[25] S. Amayri, T. Arnold, H. Foerstendorf, G. Geipel, G. Bernhard, Can. Mineral. 42 (2004) 963–972.
[26] S. Amayri, T. Arnold, T. Reich, H. Foerstendorf, G. Geipel, G. Bernhard, A. Massanek, Environ. Sci. Technol., submitted for publication.
[27] Diffracplus evaluation program, Siemens, Germany, 1999.
[28] Win-Metric: Lattice Constant Calculation Program; Robust Metric Refinement, SIGMA-C GmbH, Germany, 1997.
[29] G. Geipel, A. Brachmann, V. Brendler, G. Bernhard, H. Nitsche, Radiochim. Acta 75 (1996) 199–204.
[30] W. Matz, N. Schell, G. Bernhard, F. Prokert, T. Reich, J. Claussner, W. Oehme, R. Schlenk, S. Dienel, H. Funke, F. Eichhorn, M. Betzl, D. Pröhl, U. Strauch, G. Hüttig, H. Krug, W. Neumann, V. Brendler, P. Reichel, M.A. Denecke, H. Nitsche, J. Synchrotron Rad. 6 (1999) 1076–1085.
[31] T. Reich, G. Bernhard, G. Geipel, H. Funke, C. Hennig, A. Rossberg, W. Matz, N. Schell, H. Nitsche, Radiochim. Acta 88 (2000) 633–637.
[32] G.N. George, I.J. Pickering, EXAFSPAK: a suite of computer programs for analysis of X-ray absorption spectra, Stanford Synchrotron Radiation Laboratory, Stanford, CA, USA, 2000.
[33] S.I. Zabinsky, J.J. Rehr, A. Ankudinov, R.C. Albers, M.J. Eller, Phys. Rev. B 52 (1995) 2995–3009.
[34] H. Mayer, K. Mereiter, Tschermaks Mineral. Petrogr. Mitt. 35 (1986) 133–146.
[35] K. Mereiter, Tschermaks Mineral. Petrogr. Mitt. 30 (1982) 277–288.
[36] H.T. Evans Jr., C. Frondel, Am. Mineral. 35 (1950) 251–254.
[37] J. Cejka, Casopis Národniho Muzea—Rada Prirodovedna 148 (1979) 177–180.
[38] K. Alwan, P.A. Williams, Mineral. Mag. 43 (1980) 665–667.
[39] A. Coda, A. Della Giusta, V. Tazzoli, Acta Crystallogr. B 37 (1981) 1496–1500.
[40] K. Mereiter, Anz. Oesterr. Akad. Wiss. Math.-Naturwiss. Kl. 3 (1986) 39–41.
[41] K. Mereiter, Neues Jahrb. Mineral., Monatsh. 1986 (1986) 481–492.

[42] E.A. Hudson, P.G. Allen, L.J. Terminello, M.A. Denecke, T. Reich, Phys. Rev. B 54 (1996) 156–165.
[43] B.K. Teo, EXAFS: Basic Principles and Data Analysis, Springer-Verlag, Berlin, 1986.
[44] M.Z. Hoffman, F. Bolletta, L. Moggi, G.L. Hug, Phys. Chem. Ref. Data 18 (1989) 219–543.
[45] J.T. Bell, R.E. Biggers, J. Mol. Spectrosc. 25 (1968) 312–329.
[46] L.H. Jones, Spectrochim. Acta XV (1959) 409–411.
[47] J.R. Bartlett, R.P. Cooney, J. Mol. Struct. 193 (1989) 295–300.
[48] Y.A. Teterin, A.Y. Teterin, Russ. Chem. Rev. 73 (2004) 541–580.
[49] V.I. Nefedov, Y.A. Teterin, T. Reich, H. Nitsche, Dokl. Akad. Nauk 348 (1996) 634–636.
[50] S. Amayri, V. Brendler, G. Geipel, G. Bernhard, in preparation.